ARTICLE

Plasmon−Phonon Coupling in Electrostatically Gated β-Ga$_2$O$_3$ Films with Mobility Exceeding 200 cm^2 V^{-1} s^{-1}

Anil Kumar Rajapitamahuni,* Anusha Kamath Manjeshwar, Avinash Kumar, Animesh Datta, Praneeth Ranga, Laxman Raju Thoutam, Sriram Krishnamoorthy, Uttam Singisetti,* and Bharat Jalan*

Cite This: https://doi.org/10.1021/acsnano.1c09535

Read Online

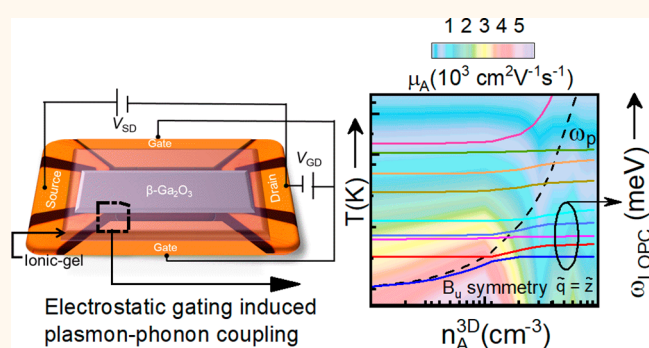ACCESS | lil Metrics & More | Article Recommendations | SI Supporting Information

ABSTRACT: Monoclinic β-Ga$_2$O$_3$, an ultra-wide bandgap semiconductor, has seen enormous activity in recent years. However, the fundamental study of the plasmon−phonon coupling that dictates electron transport properties has not been possible due to the difficulty in achieving higher carrier density (without introducing chemical disorder). Here, we report a highly reversible, electrostatic doping of β-Ga$_2$O$_3$ films with tunable carrier densities using ion-gel-gated electric double-layer transistor configuration. Combining temperature-dependent Hall effect measurements, transport modeling, and comprehensive mobility calculations using *ab initio* based electron−phonon scattering rates, we demonstrate an increase in the room-temperature mobility to 201 cm^2 V^{-1} s^{-1} followed

by a surprising decrease with an increasing carrier density due to the plasmon−phonon coupling. The modeling and experimental data further reveal an important "antiscreening" (of electron−phonon interaction) effect arising from dynamic screening from the hybrid plasmon−phonon modes. Our calculations show that a significantly higher room-temperature mobility of 300 cm^2 V^{-1} s^{-1} is possible if high electron densities (>10^{20} cm^{-3}) with plasmon energies surpassing the highest energy LO mode can be realized. As Ga$_2$O$_3$ and other polar semiconductors play an important role in several device applications, the fundamental understanding of the plasmon−phonon coupling can lead to the enhancement of mobility by harnessing the dynamic screening of the electron−phonon interactions.

KEYWORDS: plasmon−phonon coupling, electrolyte gating, ultra-wide bandgap semiconductors, transport techniques, ab initio modeling

The monoclinic phase of gallium oxide (β-Ga$_2$O$_3$) has garnered tremendous interest as an ultra-wide bandgap semiconductor ($E_g \sim 4.9$ eV) due to its high thermal stability, n-type doping over a wide range, and the availability of high-quality wafer scale native substrates.[1−3] Although several groups have demonstrated β-Ga$_2$O$_3$ (hereafter, we refer to it as Ga$_2$O$_3$) based high voltage and RF devices,[4,5] the lower room-temperature electron mobilities, as compared to other wide bandgap semiconductors,[6] have significantly limited its performance. Theoretical calculations have confirmed that the intrinsic room-temperature electron mobility in Ga$_2$O$_3$ is limited by strong electron−polar optical phonon (POP) scattering arising from the 12 IR active phonons.[7−10] Efforts to enhance the free carrier screening of the POP interaction by increasing carrier concentrations via chemical doping have resulted in the decrease of mobility due to the enhanced ionized impurity scattering.[2,11] Heterostructures where free carriers are spatially separated from the donors in modulation

doping configuration have not yielded the expected values,[12,13] possibly due to the residual impurity scattering and rough interfaces. Alternatively, electrostatic doping can be used to increase carrier density without further introducing disorder in channel materials.[14]

Recently, using ionic liquids or gels in electric double-layer transistor (EDLT) configuration, carrier densities of up to ~10^{15} cm^{-2} have been achieved in complex oxides.[15,16] These carrier densities are shown to be sizable to induce electronic phase transitions,[17] insulator−metal transitions,[18] and super-

conductivity[19,20] and alter magnetic ground states.[21] These electrostatically induced carrier densities can also be large enough to screen the POP modes in Ga_2O_3. In this article, we report the experimental observation of this effect combined with theoretical calculations showing a significant increase in the electron mobilities in ion-gel-gated Ga_2O_3 films. Gate-voltage-dependent resistance characterization reveals a wide voltage window for reversible electrostatic doping of Ga_2O_3 without any redox reactions. Hall effect measurements are performed to study the effect of electrostatic doping on the carrier mobilities, which show an enhancement with electron doping at all temperatures. A careful deconvolution of accumulation layer parameters by combining two-channel conduction model with the Thomas−Fermi (TF) approximation reveals an unusual dependence of electron mobilities on the electrostatically induced carrier densities. The mobilities increase initially and then decrease with further increase of carrier densities in the accumulation layer. This trend was observed over a large range of temperatures. A high room-temperature mobility of 201 cm^2 V^{-1} s^{-1} was observed at a carrier density of 2.24×10^{17} cm^{-3} in the accumulation layer. We further investigated the low-field electron mobilities in the accumulation layers by solving the Boltzmann transport equation (BTE) incorporating *ab initio* calculated electron−phonon interaction and plasmon−phonon coupling. The collective oscillations of the free electrons (plasmons) are well-known to couple to longitudinal phonon modes in polar semiconductors,[22−24] with experimental observation of the same.[25] Our calculations show the critical role of plasmon−phonon coupling in interpreting the mobility in ion-gel-gated Ga_2O_3 films, also revealing the long predicted "antiscreening" of phonons.[26,27]

RESULTS AND DISCUSSION

We characterized the electron transport properties of thin-film Hall bar devices of both unintentionally doped (UID) and Si-doped samples. For clarity, we will only show the measurements on the UID sample in the main text. Results from Si-doped samples are included in the Supporting Information (Figures S1 and S2). In Figure 1a, the carrier density determined by Hall effect measurements as a function of inverse temperature is plotted. We have estimated the donor concentration (N_D), acceptor concentration (N_A), and donor activation energy (E_D) values by fitting the experimentally obtained electron density (n) using the charge-neutrality equation:[28]

$$\frac{n(n + N_A)}{N_D - N_A - n} = \frac{N_C}{2}\exp\left(-\frac{E_D}{k_B T}\right) \qquad (1)$$

where N_C is the effective conduction band density of states, k_B is Boltzmann constant, and T is temperature in Kelvin. The best fit N_D, N_A, and E_D values are 3.8×10^{16} cm^{-3}, 1.5×10^{15} cm^{-3}, and 36 meV, respectively. The extracted E_D value from the fit is in good agreement with previously reported values.[29,30] The low compensation ratio (N_A/N_D) indicates the high quality of the thin films.

Figure 1b shows the Hall mobility as a function of temperature. These films show high room-temperature mobilities of 168 cm^2 V^{-1} s^{-1} that increase to 4150 cm^2 V^{-1} s^{-1} as the temperature decreases to 50 K. To quantify the role of various scattering mechanisms in our thin films, the mobility of the device is first modeled as a function of temperature (see
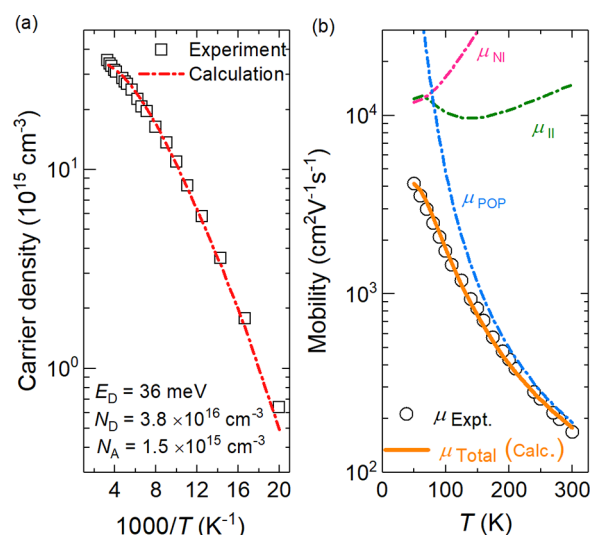

Figure 1. Temperature-dependent electron transport properties of UID β-Ga_2O_3 thin films. (a) Carrier density as a function of inverse temperature. Open square symbols are the experimental data, and the dashed line is the fit obtained from charge-neutrality equation. (b) Hall mobility as a function of temperature. Open circles are the experimental data and lines are the theoretically calculated values for specific scattering mechanisms. Here μ_{NI}, μ_{II}, and μ_{POP} are neutral impurity-, ionized impurity-, and polar-optical phonon-limited mobilities, respectively. The total mobility is calculated using Rode's iterative method.

Supporting Information for details). We treated the ionized impurity scattering considering the partial ionization of dopants with temperature. Debye screening is assumed where the effective screening electron density $(n*)$ is given by[9]

$$n* = n + \frac{(N_D - n - N_A)(n + N_A)}{N_D} \qquad (2)$$

where n is the ionized electron density at a given temperature. Figure 1b shows the electron mobility due to individual scattering mechanisms along with the total drift mobility calculated by solving the BTE using Rode's iterative method. The mobility values are in good agreement with those from the experiment for UID (Figure 1b) and Si-doped samples (Supporting Information, Figure S2). The obtained parameters from these calculations are later used to calculate the field effect mobilities when the ion-gel-gating is used, which we describe next.

Ion-gels are placed as shown in Figure 2a,b on the channel area and gate electrodes to form EDLTs. As the electrolyte contains mobile ions, a gate voltage (V_g) window therefore exists beyond which unavoidable migration of ions at the electrolyte/semiconductor interface occurs, leading to electrochemical phenomena such as intercalation and even irreversible redox chemistry.[31,32] A reversible electrostatic window of ±3 V is determined by charging and discharging the EDL capacitor at Ga_2O_3/ion-gel interface and monitoring the sheet resistance $R_\square$ (Supporting Information, Figures S3−S5). Having established the electrolyte gating mechanism in our Ga_2O_3 EDLTs, we now discuss the electrostatic doping-dependent transport properties as a function of temperature. For these measurements, a voltage pulse was applied at 270 K, and after waiting 20 min to allow sufficient time for ion movement and for charging the EDL capacitor, the sample was
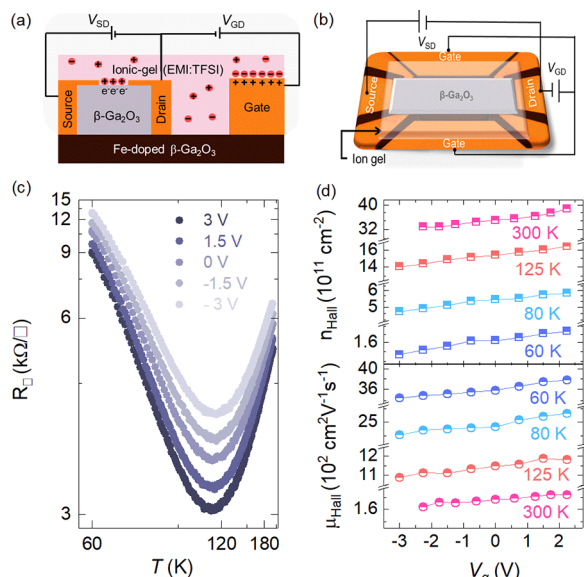
Figure 2. Ion-gel-gating studies of UID β-Ga$_2$O$_3$ thin films. (a) Schematic of an ion-gel-gated β-Ga$_2$O$_3$ thin-film structure illustrating the formation of EDL at the β-Ga$_2$O$_3$ film/ion gel interface. (b) Optical image of the fabricated Hall bar device for ion gel gating, with false color used for Ga$_2$O$_3$ channel and of ion gel. (c) Temperature-dependent sheet resistance ($R_\square$) of 1 μm-thick UID β-Ga$_2$O$_3$ as a function of V_g. (d) Corresponding gate voltage dependence of 2D Hall carrier densities (n_H) and mobilities (μ_H) at select temperatures.

then cooled down to 60 K and measurements were performed during the warming.

Figure 2 shows the $R_\square(T)$ plots at select V_g values, along with V_g dependence of Hall carrier densities (n_H) and mobilities (μ_H) at select temperatures. At $V_g = 0$ V, as temperature increases, $R_\square(T)$ follows a thermally activated behavior until ~115 K, above which it again increases due to decrease in mobility (Figure 2c). Application of $V_g = \pm 3$ V then results in modulation of $R_\square(T)$, in accordance with electron accumulation and depletion mechanisms, respectively. The relatively modest changes (~20%) observed in $R_\square(T)$ with application of V_g are due to the large thickness of the films which allows for current shunting by the bulk of the film. We chose to show $R_\square(T)$ in Figure 2c only until 200 K, as the leakage associated with the glass transition in the ion gel sets in for 200 K $\leq T \leq$ 260 K (Figure S4). We however note that the leakage current through the ion-gel is still insignificant (<50 nA) at all temperatures in the voltage range reported and, therefore, does not affect the accuracy of our transport measurements.

Figure 2d shows the V_g dependence of n_H and μ_H at select temperatures. At all temperatures, n_H increases with positive V_g due to additional accumulation of electrons and application of negative V_g leads to a decrease in n_H, consistent with the depletion picture. The corresponding values of μ_H increase monotonically with increasing V_g, at all temperatures. At room temperature, the measured mobility values increase from 161.4 cm^2 V^{-1} s^{-1} at $V_g = -2.25$ V to 168.2 cm^2 V^{-1} s^{-1} at +2.25 V, implying an enhancement in mobility with carrier density. Again, the modest V_g-induced changes in n_H and μ_H are due to the large thickness of the films. Still, the $\mu_H(V_g)$ results imply the mobilities increase with increasing carrier densities. This is in stark contrast with the chemical doping results obtained for

Ga$_2$O$_3$ thin films and single crystals, where μ_H decreases with increasing doping density. While the measured mobility increases with accumulated carriers, the values do not accurately reflect the true electrostatic modulation in the accumulation layer.

In the presence of initial chemical doping, the transport properties of the modulated layer can be separated from the bulk by applying a discrete two-channel conduction model.[33,34] Here, we focus our studies to positive gate voltages as they lead to electron accumulation and hence mobility enhancement. The two-channel model assumes that the film can be divided into two layers along the thickness of the film (z): the accumulation layer (subscript A) and the bulk layer (subscript B). The layers have z-independent effective 3D carrier densities n_i^{3D} and mobilities μ_i over their respective thicknesses d_i (i = A, B), as shown schematically in Figure 3a. The
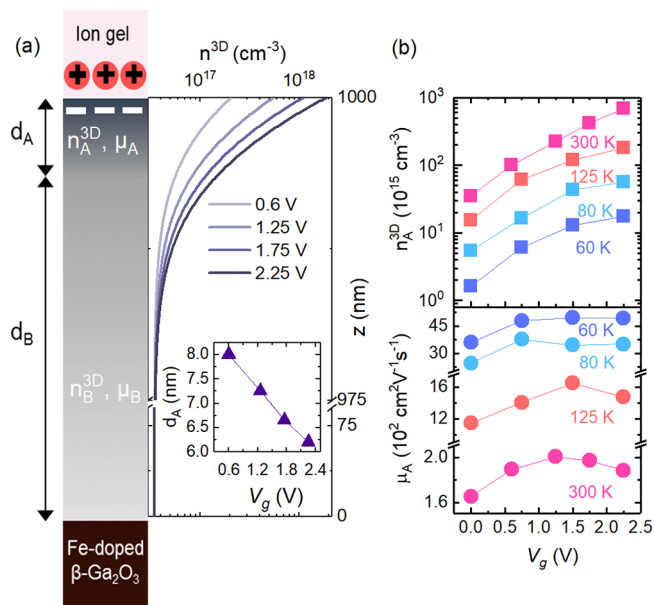

Figure 3. (a) Schematic illustration of two-channel conduction model along with 3D carrier density profiles along the thickness of a 1 μm-thick ion-gel-gated UID β-Ga$_2$O$_3$ thin film (n^{3D} vs z) for various V_g at 300 K. Inset shows the corresponding calculated accumulation layer thickness d_A as a function of V_g. (b) The corresponding gate voltage dependence of accumulation layer carrier densities (n_A^{3D}) and mobilities (μ_A) at various temperatures.

conductivity and Hall coefficients in this two-channel conduction model are given by

$$n_H \mu_H = n_A^{3D} \mu_A d_A + n_B^{3D} \mu_B d_B \qquad (3)$$

$$n_H \mu_H^2 = n_A^{3D} \mu_A^2 d_A + n_B^{3D} \mu_B^2 d_B \qquad (4)$$

where n_H and μ_H are the measured Hall sheet carrier density and mobility values (Figure 2d), and $z = d_A + d_B$. The bulk region with thickness d_B is assumed to retain properties identical to those at $V_g = 0$, that is, $n_B^{3D} = n^{3D}(V_g = 0) = \frac{n_H}{z}$ and $\mu_B = \mu_H (V_g = 0)$. Extraction of n_A^{3D} and μ_A from eqs 3 and 4, therefore, requires an estimation of d_A.

The accumulation layer thickness d_A can be determined from depth profile of charge density (ρ_c). The charge density is a function of induced 3D carrier density ($n^{3D} - n_B^{3D}$) and is related to the electric potential φ via the Poisson equation:

$$\frac{d^2\varphi}{dz^2} = -\frac{\rho_c}{\kappa\varepsilon_0} = -\frac{(-e)(n^{3D} - n_B^{3D})}{\kappa\varepsilon_0} \tag{5}$$

where κ is the dielectric constant and ε_0 the vacuum permittivity. To solve the above equation for $n^{3D}(z)$, we employ the TF approximation[35] that relates n^{3D} and φ with the relation:

$$\varphi(z) = (3\pi^2 n^{3D}(z))^{2/3}\left(\frac{\hbar^2}{2m_e^* e}\right) \tag{6}$$

where m_e^* is the electron effective mass. Depth-dependent electrostatically induced potential profiles $\varphi(z)$ and electron distributions $n^{3D}(z)$ for various V_g's can be obtained by combining eqs 5 and 6 with appropriate boundary conditions (Supporting Information, Figure S7). Here, we note that, as TF approximation treats electrons in the accumulation layer as 3D free electron gas, its validity requires $k_F d_A > 1$, where $k_F = (3\pi^2 n_A^{3D})^{1/3}$ is the Fermi wave vector.[34] For an average value of $d_A \approx 6.5$ nm, for both the films, the above condition is valid.

Figure 3a shows $n^{3D}(z)$ at 300 K for various gate voltages. Here, $z = 0$ corresponds to substrate/Ga$_2$O$_3$ interface, while $z = 1000$ nm corresponds to ion gel/Ga$_2$O$_3$ interface, and $n^{3D}(z)$ approaches the initial chemical doping levels for all V_g, away from the interface, inside the bulk of the thin film. Toward the Ga$_2$O$_3$/ion gel interface, $n^{3D}(z)$ differs, increasing with V_g. A d_A value is then determined from these $n^{3D}(z)$ profiles, which we define as the thickness over which 90% of electrostatically charged induced electrons are confined, similar to ref 36. The extracted d_A vs V_g at 300 K is plotted in the inset of Figure 3a. The d_A decreases with V_g due to higher confinement by the gate-induced electric fields at the Ga$_2$O$_3$/ion gel interface. These values of d_A are then used in eqs 3 and 4 to determine n_A^{3D} and μ_A. In Figure 3b,c, V_g-dependent n_A^{3D} and μ_A at various temperatures are plotted. At all temperatures n_A^{3D} increases with increase in V_g (Figure 3b). On the other hand, $\mu_A(V_g)$ initially increases at low V_g at all temperatures. A further increase of V_g results in saturation of μ_A at low temperatures, while at high temperatures, μ_A decreases with V_g even though the corresponding n_A^{3D} is still increasing. Regardless, we measured a high mobility of 201 cm^2 V^{-1} s^{-1} for $V_g = 1.25$ V at 300 K, which is comparable to the best reported mobilities in Ga$_2$O$_3$. Here we note that d_A is determined assuming flat band conditions and TF approximation, which is valid for degenerate semiconductors with Fermi surfaces. Therefore, we have performed error analysis (Supporting Information, Figure S8) assuming different confinement depths for induced carriers and also calculated d_A using the Debye screening model. This analysis resulted in only a slight variation of mobilities from 194 to 202 cm^2 V^{-1} s^{-1} for $V_g = 1.25$ V at 300 K.

To better understand the mobility trends with V_g, we replot μ_A, as a function of the accumulation layer carrier density, n_A^{3D}, as shown in Figure 4a. At all T, μ_A increases initially with increased electron doping, consistent with the improved screening of ionized impurities and/or charged defects, as observed in polarization doped AlGaN films.[37] However, at higher doping densities, $\mu_A(n_A^{3D})$ shows a dip even though one would expect the mobility to further increase due to enhanced screening. Kang et al.,[8] by considering static screening of electron phonon interactions, have shown, theoretically, a decrease in the Hall mobility at $\sim 10^{20}$ cm^{-3} after an initial increase from 10^{17} to 10^{19} cm^{-3}, which they attribute to free
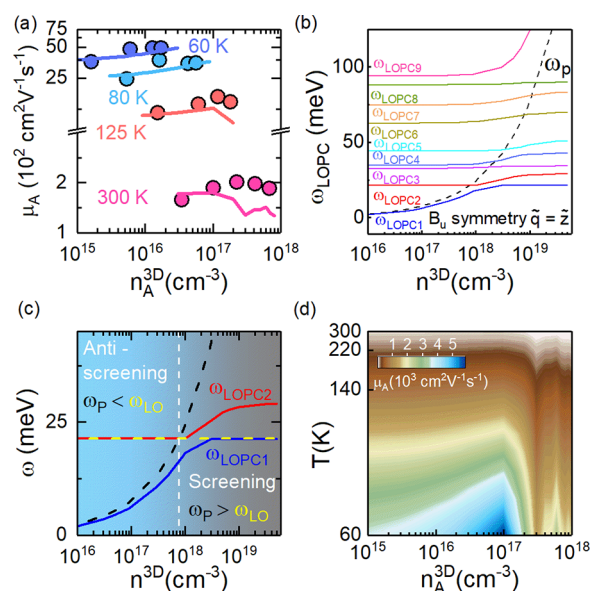

Figure 4. (a) Mobilities (μ_A) vs electrostatic induced carrier densities (n_A^{3D}) in the accumulation layer. Filled circles are experimental data and lines are mobilities obtained via DFT calculations including LOPC. Effect of plasmon−phonon coupling on field effect mobilities in UID β-Ga$_2$O$_3$. (b) The B_u symmetry LOPC modes as a function of electron concentrations for the wave vector along the z direction. The pure plasmon mode is shown as a black dashed line. (c) Screening and antiscreening of LO phonons by plasmons depending on carrier densities. (d) Contour plot of field effect mobilities as a function of electrostatic doping densities for various temperatures.

carrier screening becoming less effective at high carrier densities. However, the observed decrease in our mobility values occurs at $\sim 10^{17}$ cm^{-3}, orders of magnitude less.

To gain more insight on the non-monotonic behavior in μ_A (n_A^{3D}), we calculate the mobility in the accumulation layer by solving the BTE, as described in Supporting Information. The Debye screening is again assumed to screen the ionized impurities where the effective screening electron density (n^{3D}) is now modified to include the ion-gel-gating enhanced electron density (n_A^{3D}) as

$$n^{3D} = n^* + n_A^{3D}$$

As the accumulation carrier density increases, the collective oscillations plasmon energy ($\omega_P^2 = \frac{\hbar^2 n^{3D} e^2}{m^* \varepsilon_\infty}$) increases. As described in the beginning of this article, the plasmon couples with the longitudinal optical phonons in polar Ga$_2$O$_3$. These coupled modes with mixed plasmon−phonon character are referred here as longitudinal optical plasmon-phonon coupling (LOPC).[23,24,38] Although frequently ignored in transport studies to simplify calculations, the coupled modes are expected to impact the carrier transport.[27,39,40] Direct observation of the coupled LOPC modes in GaAs[25] and in graphene on SiC and SiO$_2$,[41−43] which agree with theoretical calculations, further give credence to the importance of the LOPC modes in doped films. The screening of the electron−phonon scattering by plasmons is a complex process which can either enhance (antiscreen) or decrease (screen) the electron−phonon scattering. This dynamic screening resulting from the plasmon−phonon coupling and its impact on carrier transport has been extensively studied in other semiconductors, namely,

Si, III-Vs, and MoS_2.[22,40,44−49] Recently, spectroscopic ellipsometry experiments have shown the presence of plasmon−phonon coupling in Ga_2O_3.[50,51]

Figure 4b shows the calculated LOPC modes in Ga_2O_3 using the plasmon-pole approximation, covering the electron concentrations that have been achieved in our gating experiments. In a large unit cell polar semiconductor Ga_2O_3, the dynamic screening is complicated by presence of multiple POP modes. At a certain electron density, coupling between the plasmons and LO phonons results in multiple LOPC frequencies out of which two are shown in Figure 4c, along with an LO mode of lowest energy for the purpose of illustration. When the plasmon energy reaches LO mode energy but is less than the LO energy, it antiscreens the mode enhancing the phonon scattering strength which would translate into decrease in the mobility. In contrast, when the plasmon energy becomes higher than that of the given LO mode energy, the former screens the latter and enhances the mobility. For Ga_2O_3, which has multiple LO modes present, this process is more complex. At a given electron density, few of the modes will be screened and a few will be antiscreened depending on their energy, thus the corresponding mobility shows a non-monotonic behavior with the change in electron density by electrostatic doping. This is plotted for various temperatures for the UID sample in a contour plot in Figure 4d. For all temperatures shown, the mobility first increases due to the Debye screening of ionized impurities, where the concentration of impurities remains constant, while the electron density (n_A^{3D}) in the channel increases with ion gel gating. The LOPC starts to appear around $\sim 10^{17}$ cm^{-3}, and as explained, the mobility starts showing a non-monotonic trend starting with a decrease in mobility as the electron density is further increased, which is attributed to the antiscreening of LO phonons. This non-monotonic behavior is expected until the plasmon energy is higher than the highest LO mode, after which only an increasing trend in the mobility is observed with the mobility of 300 cm^2 V^{-1} s^{-1} expected at a carrier density of $\sim 10^{20}$ cm^{-3} (Supporting Information, Figure S9).

In Figure 4a, the calculated total mobility with electron density is compared with the experimentally obtained data. At very low temperature (60 and 80 K), the electron density is not high enough (see Figure 4d) for the LOPC to come into the picture, and hence, an increasing trend is observed that is due to the Debye screening as explained before. At higher temperatures, mobility first increases with n_A^{3D} as expected, then beyond $\sim 10^{17}$ cm^{-3}, the mobility starts to decrease. We attribute this to the antiscreening of the phonons. The calculated mobility values match reasonably well with the experimental data across the range of doping densities and temperatures. It is noted that we have calculated the surface roughness scattering and found it negligible compared to other mechanisms. Thus, the observed features are signatures of antiscreening arising from the plasmon−phonon modes. A slight discrepancy in the calculated and experimental values at 300 K could be due to the deviation of Hall scattering factor from 1 at these temperatures, the use of zero-Kelvin plasmon polarizability function in our calculations, and assuming zero damping of the plasmon−phonon modes. A similar behavior is also seen in Si-doped Ga_2O_3 sample (Supporting Information, Figure S8). Nevertheless, these findings confirm the mobilities in our ion-gel-gated devices are limited by LOPC. Although, plasmon−phonon mode coupling in Ga_2O_3 has been previously reported in single crystals,[50,51] our experiments

clearly show the effects of their dynamical screening on the electron mobilities in the absence of intentional impurities in thin films. These results show achieving high electron densities with plasmon energies surpassing highest energy LO mode could potentially be used to improve the low mobilities in Ga_2O_3 (Supporting Information, Figure S9).

Finally, we compare in Figure 5 the room-temperature mobilities at various carrier densities for previously reported
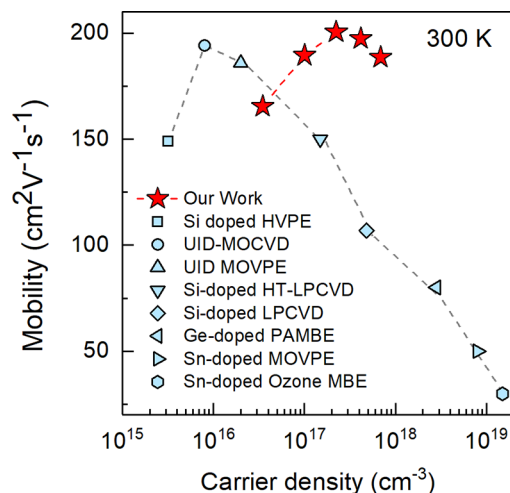

Figure 5. Comparison of room-temperature electron mobilities in high crystalline epitaxial thin films of β-Ga_2O_3 as a function of carrier concentrations achieved via chemical doping to that obtained via electrostatic doping from this work. The blue, solid symbols show experimental results from various groups: ■, ref 54; ●, ref 59; ▲, ref 60; ▼, ref 58; ♦, ref 52; left-pointing triangle, ref 55; right-pointing triangle, ref 56; and ◆ ref 57, and the red star symbols (★) are data from this work. The dashed lines are a guide to the eye.

state-of-the-art thin films[11,52−60] of Ga_2O_3 with those obtained from our electrostatic doping experiments. While in chemical doped films where an increase of electron density leads to a decrease of mobilities, our work highlights a reverse trend that shows an enhancement in electron mobilities with electrostatic doping. At carrier densities of $\sim 10^{18}$ cm^{-3}, the field effect mobilities in our films (~ 187 cm^2 V^{-1} s^{-1}) are a factor of ~ 2 larger than the best reported values for the highest quality chemically doped thin films. The observation of LOPC modes even with the moderate 2DEG electron densities ($\sim 5 \times 10^{11}$ cm^{-2}) achieved in our field effect experiments is encouraging enough to envision higher room-temperature mobilities in Ga_2O_3 via modulation doping, where in 2DEG densities of an order of magnitude higher than in our field effect experiments are routinely achieved.

CONCLUSIONS

We have comprehensively investigated the electron transport properties in ion-gel-gated Ga_2O_3 films. Gate-voltage-dependent resistance measurements reveal the resistance can be modulated reversibly over a wide voltage range, establishing the electrostatic nature of the doping mechanism in our field effect experiments. Hall effect measurements combined with the two-channel conduction model and Thomas−Fermi approximation reveal that gate voltage can be used to enhance mobilities with electrostatically induced electron doping. The accumulation layer carrier densities have been modulated over

an order of magnitude, with a small voltage, while the mobilities reached high values of 201 cm^2 V^{-1} s^{-1} at 300 K. High electron mobility is maintained even at an electron density of 10^{18} cm^{-3}. Transport calculations, including the first-principles electron−phonon scattering rate, show that the plasmon−phonon coupling plays a crucial role in determining the electron transport properties of Ga$_2$O$_3$ films. We also show a signature of antiscreening arising from the dynamic screening of the coupled plasmon−phonon modes.

METHODS

Homoepitaxial Si-doped and unintentionally doped (UID) Ga$_2$O$_3$ thin films of thicknesses of 1.3 and 1 μm, respectively, are grown on (010) Fe-doped semi-insulating Ga$_2$O$_3$ substrates using an Agnitron Agilis metal−organic vapor-phase epitaxy reactor. Note that thinner layers were not used to avoid potential issues related to substrate/film interface. Details of the growth are discussed in the Supporting Information and elsewhere.[60,61] For electron transport and electrolyte gating studies, Hall bar devices, with channel lengths of 720 μm and widths of 120−240 μm, are defined using photolithography and BCl$_3$/Ar-based reactive ion-etching. Metal contacts and coplanar gate electrodes are defined using a second photolithography step followed by sputtering of Ti/Au (30 nm/70 nm). Ohmic contacts are achieved by a rapid thermal annealing step at 470 °C in N$_2$ for 90 s. For ion gel gating experiments, "cut and stick" ion gels[62] formed by mixing ionic liquid (1-ethyl-3-methylimidazolium bis(trifluoromethylsulfonyl)-imide ([EMI][TFSI])) with polymer (poly(vinylidene fluoride-co-hexafluoropropylene) [P(VDF-HFP)]) in 4:1 wt % are used. The temperature-dependent Hall effect measurements are performed in a DynaCool Physical Property Measurement System (Quantum Design) using Keithley electronics. Hall resistance (R_{xy}) is measured, while magnetic fields (H) of ±2.5 T are swept, and the carrier densities are determined from the slope of the R_{xy} vs H plots, assuming a Hall factor of 1. Electrical measurements are performed using DC excitation currents of 1−5 μA.

The POP electron−phonon interactions are calculated from density functional theory (DFT) and density functional perturbation theory framework. The details of the method can be found in previous reports.[13,63] The POP scattering rate is calculated from the plasmon−phonon coupled modes. The LOPC modes are calculated using the plasmon-pole approximation,[27] followed by extracting the LO phonon contribution to each coupled mode to calculate the scattering strength. The Landau damping is considered at very high electron density, and the plasmon dispersion is ignored based on the upper boundary of electron−hole pair continuum. The POP scattering rate is known to be dominant for Ga$_2$O$_3$ at higher temperatures and the ionized impurity at low temperatures,[7,9] hence the nonpolar deformation potential scattering is omitted in our calculation. The ionized impurity and the neutral impurity scattering are included in the mobility calculations. The low field electron mobility is then calculated by solving the Boltzmann transport equation (BTE) using Rode's iterative method. The Supporting Information contains detailed information and equations pertaining to every step.

ASSOCIATED CONTENT

ⓈⒾ Supporting Information

The Supporting Information is available free of charge at https://pubs.acs.org/doi/10.1021/acsnano.1c09535.

> Details of film growth, mobility calculations by first principle DFT, gate effect and irreversibility studies, methodology to determine accumulation layer thickness, error analysis of calculated mobilities, LOPC screening at higher carrier densities, effect of phonon occupancy on the POP scattering and electron transport and gating phenomena in Si-doped Ga$_2$O$_3$ thin films like the UID sample in the manuscript (PDF)

AUTHOR INFORMATION

Corresponding Authors

Anil Kumar Rajapitamahuni − *Department of Chemical Engineering and Materials Science, University of Minnesota, Minneapolis, Minnesota 55455, United States;* Email: rajap016@umn.edu

Bharat Jalan − *Department of Chemical Engineering and Materials Science, University of Minnesota, Minneapolis, Minnesota 55455, United States;* ⓘ orcid.org/0000-0002-7940-0490; Email: bjalan@umn.edu

Uttam Singisetti − *Department of Electrical Engineering, University at Buffalo, Buffalo, New York 14260, United States;* Email: uttamsin@buffalo.edu

Authors

Anusha Kamath Manjeshwar − *Department of Chemical Engineering and Materials Science, University of Minnesota, Minneapolis, Minnesota 55455, United States*

Avinash Kumar − *Department of Electrical Engineering, University at Buffalo, Buffalo, New York 14260, United States*

Animesh Datta − *Department of Electrical Engineering, University at Buffalo, Buffalo, New York 14260, United States*

Praneeth Ranga − *Department of Electrical and Computers Engineering, The University of Utah, Salt Lake City, Utah 84112, United States*

Laxman Raju Thoutam − *Department of Chemical Engineering and Materials Science, University of Minnesota, Minneapolis, Minnesota 55455, United States;* Present Address: Department of Electronics and Communications Engineering, SR University, Warangal Urban 506371, Telangana, India

Sriram Krishnamoorthy − *Department of Electrical and Computers Engineering, The University of Utah, Salt Lake City, Utah 84112, United States; Materials Department, University of California, Santa Barbara, Santa Barbara, California 93106, United States*

Complete contact information is available at:
https://pubs.acs.org/10.1021/acsnano.1c09535

Author Contributions

A.K.R, A.K.M., and B.J. conceived the idea and designed the experiments. P.R. grew samples and characterized them structurally under the guidance of S.K. A.K.R, A.K.M., and L.R.T. performed transport measurements. A.K.M. and A.K.R. performed analysis to separate the accumulation layer carrier densities and mobilities. Mobility calculations were performed by A.K. and A.D. under the guidance of U.S. A.K.R, A.K.M., and B.J. wrote the manuscript. All authors contributed to the discussion and manuscript preparation.

Notes

ACKNOWLEDGMENTS

REFERENCES

(1) Higashiwaki, M.; Jessen, G. H. Guest Editorial: The Dawn of Gallium Oxide Microelectronics. *Appl. Phys. Lett.* **2018**, *112* (6), 060401.

(2) Zhang, J. Y.; Shi, J. L.; Qi, D. C.; Chen, L.; Zhang, K. H. L. Recent Progress on the Electronic Structure, Defect, and Doping Properties of Ga_2O_3. *APL Materials* **2020**, *8* (2), 020906.

(3) Galazka, Z. β-Ga_2O_3 for Wide-Bandgap Electronics and Optoelectronics. *Semicond. Sci. Technol.* **2018**, *33* (11), 113001.

(4) Higashiwaki, M.; Sasaki, K.; Murakami, H.; Kumagai, Y.; Koukitu, A.; Kuramata, A.; Masui, T.; Yamakoshi, S. Recent Progress in Ga_2O_3 Power Devices. *Semicond. Sci. Technol.* **2016**, *31* (3), 034001.

(5) Pearton, S. J.; Yang, J. C.; Cary, P. H.; Ren, F.; Kim, J.; Tadjer, M. J.; Mastro, M. A. A Review of Ga_2O_3 Materials, Processing, and Devices. *Applied Physics Reviews* **2018**, *5* (1), 011301.

(6) Tsao, J. Y.; Chowdhury, S.; Hollis, M. A.; Jena, D.; Johnson, N. M.; Jones, K. A.; Kaplar, R. J.; Rajan, S.; Van de Walle, C. G.; Bellotti, E.; Chua, C. L.; Collazo, R.; Coltrin, M. E.; Cooper, J. A.; Evans, K. R.; Graham, S.; Grotjohn, T. A.; Heller, E. R.; Higashiwaki, M.; Islam, M. S.; Juodawlkis, P. W.; Khan, M. A.; Koehler, A. D.; Leach, J. H.; Mishra, U. K.; Nemanich, R. J.; Pilawa-Podgurski, R. C. N.; Shealy, J. B.; Sitar, Z.; Tadjer, M. J.; Witulski, A. F.; Wraback, M.; Simmons, J. A. Ultrawide-Bandgap Semiconductors: Research Opportunities and Challenges. *Advanced Electronic Materials* **2018**, *4* (1), 1600501.

(7) Ghosh, K.; Singisetti, U. Ab initio calculation of electron-phonon coupling in monoclinic β-Ga_2O_3 crystal. *Appl. Phys. Lett.* **2016**, *109* (7), 072102.

(8) Kang, Y.; Krishnaswamy, K.; Peelaers, H.; Van de Walle, C. G. Fundamental limits on the electron mobility of β-Ga_2O_3. *J. Phys-Condens Mat* **2017**, *29* (23), 234001.

(9) Ma, N.; Tanen, N.; Verma, A.; Guo, Z.; Luo, T. F.; Xing, H.; Jena, D. Intrinsic electron mobility limits in β-Ga_2O_3. *Appl. Phys. Lett.* **2016**, *109* (21), 212101.

(10) Parisini, A.; Fornari, R. Analysis of the scattering mechanisms controlling electron mobility in β-Ga_2O_3 crystals. *Semicond. Sci. Technol.* **2016**, *31* (3), 035023.

(11) Feng, Z. X.; Bhuiyan, A. F. M. A. U.; Karim, M. R.; Zhao, H. P. MOCVD homoepitaxy of Si-doped (010) β-Ga_2O_3 thin films with superior transport properties. *Appl. Phys. Lett.* **2019**, *114* (25), 250601.

(12) Krishnamoorthy, S.; Xia, Z. B.; Joishi, C.; Zhang, Y. W.; McGlone, J.; Johnson, J.; Brenner, M.; Arehart, A. R.; Hwang, J. W.; Lodha, S.; Rajan, S. Modulation-doped beta-$(Al_{0.2}Ga_{0.8})_2O_3/Ga_2O_3$ field-effect transistor. *Appl. Phys. Lett.* **2017**, *111* (2), 023502.

(13) Kumar, A.; Ghosh, K.; Singisetti, U. Low field transport calculation of 2-dimensional electron gas in beta - $(Al_xGa_{1-x})_2O_3/Ga_2O_3$ heterostructures. *J. Appl. Phys.* **2020**, *128* (10), 105703.

(14) Goldman, A. M. Electrostatic Gating of Ultrathin Films. *Annual Review of Materials Research, Vol 44* **2014**, *44*, 45−63.

(15) Bisri, S. Z.; Shimizu, S.; Nakano, M.; Iwasa, Y. Endeavor of Iontronics: From Fundamentals to Applications of Ion-Controlled Electronics. *Adv. Mater.* **2017**, *29* (25), 1607054.

(16) Leighton, C. Electrolyte-Based Ionic Control of Functional Oxides. *Nat. Mater.* **2019**, *18* (1), 13−18.

(17) Lee, Y.; Clement, C.; Hellerstedt, J.; Kinney, J.; Kinnischtzke, L.; Leng, X.; Snyder, S. D.; Goldman, A. M. Phase Diagram of Electrostatically Doped $SrTiO_3$. *Phys. Rev. Lett.* **2011**, *106* (13), 136809 DOI: 10.1103/PhysRevLett.106.136809.

(18) Thoutam, L. R.; Yue, J.; Prakash, A.; Wang, T. Q.; Elangovan, K. E.; Jalan, B. Electrostatic Control of Insulator-Metal Transition in La-Doped $SrSnO_3$ Films. *ACS Appl. Mater. Interfaces* **2019**, *11* (8), 7666−7670.

(19) Bollinger, A. T.; Dubuis, G.; Yoon, J.; Pavuna, D.; Misewich, J.; Bozovic, I. Superconductor-Insulator Transition in $La_{2-x}Sr_xCuO_4$ at the Pair Quantum Resistance. *Nature* **2011**, *472* (7344), 458−460.

(20) Leng, X.; Garcia-Barriocanal, J.; Bose, S.; Lee, Y.; Goldman, A. M. Electrostatic Control of the Evolution from a Superconducting Phase to an Insulating Phase in Ultrathin $YBa_2Cu_3O_{7-x}$ Films. *Phys. Rev. Lett.* **2011**, *107* (3), 039901 DOI: 10.1103/PhysRevLett.107.039901.

(21) Walter, J.; Voigt, B.; Day-Roberts, E.; Heltemes, K.; Fernandes, R. M.; Birol, T.; Leighton, C. Voltage-Induced Ferromagnetism in a Diamagnet. *Sci. Adv.* **2020**, *6* (31), abb7721.

(22) Peeters, F. M.; Wu, X. G.; Devreese, J. T. Coupled Plasmon-Lo-Phonon Modes in Gax In1-X as Heterostructures. *Phys. Rev. B* **1987**, *36* (14), 7518−7522.

(23) Varga, B. B. Coupling of Plasmons to Polar Phonons in Degenerate Semiconductors. *Phys. Rev.* **1965**, *137* (6A), 1896.

(24) Yokota, I. On Coupling between Optical Lattice Vibrations and Carrier Plasma Oscillations in Polar Semiconductors. *J. Phys. Soc. Jpn.* **1961**, *16* (10), 2075.

(25) Mooradian, A.; Wright, G. B. Observation of the Interaction of Plasmons with Longitudinal Optical Phonons in GaAs. *Phys. Rev. Lett.* **1966**, *16* (22), 999−1001.

(26) Fischetti, M. V.; Laux, S. E. Monte Carlo study of electron transport in silicon inversion layers. *Phys. Rev. B* **1993**, *48* (4), 2244−2274.

(27) Hauber, A.; Fahy, S. Scattering of carriers by coupled plasmon-phonon modes in bulk polar semiconductors and polar semiconductor heterostructures. *Phys. Rev. B* **2017**, *95* (4), 045210.

(28) Yu, P. Y.; Cardona, M. Fundamentals of Semiconductors: Physics and Materials Properties, Fourth Edition. *Fundamentals of Semiconductors: Physics and Materials Properties, Fourth Edition* **2010**, 1−775.

(29) Irmscher, K.; Galazka, Z.; Pietsch, M.; Uecker, R.; Fornari, R. Electrical properties of beta-Ga2O3 single crystals grown by the Czochralski method. *J. Appl. Phys.* **2011**, *110* (6), 063720.

(30) Neal, A. T.; Mou, S.; Rafique, S.; Zhao, H. P.; Ahmadi, E.; Speck, J. S.; Stevens, K. T.; Blevins, J. D.; Thomson, D. B.; Moser, N.; Chabak, K. D.; Jessen, G. H. Donors and deep acceptors in β-Ga_2O_3. *Appl. Phys. Lett.* **2018**, *113* (6), 062101.

(31) Chodankar, N. R.; Pham, H. D.; Nanjundan, A. K.; Fernando, J. F. S.; Jayaramulu, K.; Golberg, D.; Han, Y. K.; Dubal, D. P. True Meaning of Pseudocapacitors and Their Performance Metrics: Asymmetric versus Hybrid Supercapacitors. *Small* **2020**, *16* (37), 2002806.

(32) Walter, J.; Wang, H. L.; Luo, B.; Frisbie, C. D.; Leighton, C. Electrostatic versus Electrochemical Doping and Control of Ferromagnetism in Ion-Gel-Gated Ultrathin $La_{0.5}Sr_{0.5}CoO_3$-delta. *ACS Nano* **2016**, *10* (8), 7799−7810.

(33) Arnaudov, B.; Paskova, T.; Evtimova, S.; Valcheva, E.; Heuken, M.; Monemar, B. Multilayer Model for Hall Effect Data Analysis of Semiconductor Structures with Step-Changed Conductivity. *Phys. Rev. B* **2003**, *67* (4), 045314.

(34) Reich, K. V.; Schecter, M.; Shklovskii, B. I. Accumulation, Inversion, and Depletion Layers in $SrTiO_3$. *Phys. Rev. B* **2015**, *91* (11), 115303.

(35) Petritz, R. L. Theory of an Experiment for Measuring the Mobility and Density of Carriers in the Space-Charge Region of a Semiconductor Surface. *Phys. Rev.* **1958**, *110* (6), 1254−1262.

(36) Wang, H.; Walter, J.; Ganguly, K.; Yu, B. Q.; Yu, G. C.; Zhang, Z.; Zhou, H.; Fu, H.; Greven, M.; Leighton, C. Wide-Voltage-Window Reversible Control of Electronic Transport in Electrolyte-Gated Epitaxial $BaSnO_3$. *Physical Review Materials* **2019**, *3* (7), 075001.

(37) Zhu, M. D.; Qi, M.; Nomoto, K.; Hu, Z. Y.; Song, B.; Pan, M.; Gao, X.; Jena, D.; Xing, H. G. Electron Mobility in Polarization-Doped $Al_{0-0.2}GaN$ with a Low Concentration Near 10^{17} cm^{-3}. *Appl. Phys. Lett.* **2017**, *110* (18), 182102.

(38) Singwi, K. S.; Tosi, M. P. Interaction of Plasmons and Optical Phonons in Degenerate Semiconductors. *Phys. Rev.* **1966**, *147* (2), 658.

(39) Kim, M. E.; Das, A.; Senturia, S. D. Electron Scattering Interaction with Coupled Plasmon-Polar-Phonon Modes in Degenerate Semiconductors. *Phys. Rev. B* **1978**, *18* (12), 6890−6899.

(40) Fischetti, M. V.; Neumayer, D. A.; Cartier, E. A. Effective Electron Mobility in Si Inversion Layers in Metal-Oxide-Semiconductor Systems with a High-Kappa Insulator: The Role of Remote Phonon Scattering. *J. Appl. Phys.* **2001**, *90* (9), 4587−4608.

(41) Koch, R. J.; Seyller, T.; Schaefer, J. A. Strong Phonon-Plasmon Coupled Modes in the Graphene/Silicon Carbide Heterosystem. *Phys. Rev. B* **2010**, *82* (20), 201413.

(42) Liu, Y.; Willis, R. F. Plasmon-Phonon Strongly Coupled Mode in Epitaxial Graphene. *Phys. Rev. B* **2010**, *81* (8), 081406.

(43) Luxmoore, I. J.; Gan, C. H.; Liu, P. Q.; Valmorra, F.; Li, P.; Faist, J.; Nash, G. R. Strong Coupling in the Far-Infrared between Graphene Plasmons and the Surface Optical Phonons of Silicon Dioxide. *ACS Photonics* **2014**, *1* (11), 1151−1155.

(44) Ahn, S.; Hwang, E. H.; Min, H. Inelastic Carrier Lifetime in a Coupled Graphene/Electron-Phonon System: Role of Plasmon-Phonon Coupling. *Phys. Rev. B* **2014**, *90* (24), 245436.

(45) Artus, L.; Cusco, R.; Ibanez, J.; Blanco, N.; Gonzalez-Diaz, G. Raman Scattering by LO Phonon-Plasmon Coupled Modes in n-type InP. *Phys. Rev. B* **1999**, *60* (8), 5456−5463.

(46) Hauber, A.; Fahy, S. Scattering of Carriers by Coupled Plasmon-Phonon Modes in Bulk Polar Semiconductors and Polar Semiconductor Heterostructures. *Phys. Rev. B* **2017**, *95* (4), 045210.

(47) Klein, M. V.; Colwell, P. J.; Ganguly, B. N. Theoretical and Experimental Study of Raman Scattering from Coupled LO-Phonon-Plasmon Modes in Silicon-Carbide. *Phys. Rev. B* **1972**, *6* (6), 2380.

(48) Olson, C. G.; Lynch, D. W. Longitudinal-Optical-Phonon-Plasmon Coupling in GaAs. *Phys. Rev.* **1969**, *177* (3), 1231.

(49) Xiaoguang, W.; Peeters, F. M.; Devreese, J. T. Plasmon-Phonon Coupling in a Two-Dimensional Electron-Gas. *Phys. Rev. B* **1985**, *32* (10), 6982−6985.

(50) Schubert, M.; Korlacki, R.; Knight, S.; Hofmann, T.; Schoche, S.; Darakchieva, V.; Janzen, E.; Monemar, B.; Gogova, D.; Thieu, Q. T.; Togashi, R.; Murakami, H.; Kumagai, Y.; Goto, K.; Kuramata, A.; Yamakoshi, S.; Higashiwaki, M. Anisotropy, phonon modes, and free charge carrier parameters in monoclinic beta-gallium oxide single crystals. *Phys. Rev. B* **2016**, *93* (12), 125209.

(51) Schubert, M.; Mock, A.; Korlacki, R.; Knight, S.; Galazka, Z.; Wagner, G.; Wheeler, V.; Tadjer, M.; Goto, K.; Darakchieva, V. Longitudinal phonon plasmon mode coupling in β-Ga_2O_3. *Appl. Phys. Lett.* **2019**, *114* (10), 102102.

(52) Rafique, S.; Han, L.; Neal, A. T.; Mou, S.; Boeckl, J.; Zhao, H. Towards High-Mobility Heteroepitaxial β-Ga_2O_3 on Sapphire - Dependence on The Substrate Off-Axis Angle. *Physica status solidi (a)* **2018**, *215* (2), 1700467.

(53) Zhang, Y. W.; Alema, F.; Mauze, A.; Koksaldi, O. S.; Miller, R.; Osinsky, A.; Speck, J. S. MOCVD Grown Epitaxial β-Ga_2O_3 Thin Film with an Electron Mobility of 176 cm^2/Vs at Room Temperature. *APL Mater.* **2019**, *7* (2), 022506.

(54) Goto, K.; Konishi, K.; Murakami, H.; Kumagai, Y.; Monemar, B.; Higashiwaki, M.; Kuramata, A.; Yamakoshi, S. Halide Vapor Phase Epitaxy of Si Doped β-Ga_2O_3 and its Electrical Properties. *Thin Solid Films* **2018**, *666*, 182−184.

(55) Ahmadi, E.; Koksaldi, O. S.; Kaun, S. W.; Oshima, Y.; Short, D. B.; Mishra, U. K.; Speck, J. S. Ge Doping of β-Ga_2O_3 Films Grown by Plasma-Assisted Molecular Beam Epitaxy. *Applied Physics Express* **2017**, *10* (4), 041102.

(56) Baldini, M.; Albrecht, M.; Fiedler, A.; Irmscher, K.; Schewski, R.; Wagner, G. Editors' Choice—Si- and Sn-Doped Homoepitaxial β-Ga_2O_3 Layers Grown by MOVPE on (010)-Oriented Substrates. *Ecs J. Solid State Sc* **2017**, *6* (2), Q3040−Q3044.

(57) Sasaki, K.; Kuramata, A.; Masui, T.; Víllora, E. G.; Shimamura, K.; Yamakoshi, S. Device-Quality β-Ga_2O_3 Epitaxial Films Fabricated by Ozone Molecular Beam Epitaxy. *Appl. Phys. Express* **2012**, *5* (3), 035502.

(58) Zhang, Y.; Feng, Z.; Karim, M. R.; Zhao, H. High-Temperature Low-Pressure Chemical Vapor Deposition of β-Ga_2O_3. *Journal of Vacuum Science & Technology A* **2020**, *38* (5), 050806.

(59) Feng, Z.; Bhuiyan, A. F. M. A. U.; Xia, Z.; Moore, W.; Chen, Z.; McGlone, J. F.; Daughton, D. R.; Arehart, A. R.; Ringel, S. A.; Rajan, S.; Zhao, H. Probing Charge Transport and Background Doping in Metal-Organic Chemical Vapor Deposition-Grown (010) β-Ga_2O_3. *Physica status solidi (RRL) - Rapid Research Letters* **2020**, *14* (8), 2000145.

(60) Bhattacharyya, A.; Ranga, P.; Roy, S.; Ogle, J.; Whittaker-Brooks, L.; Krishnamoorthy, S. Low Temperature Homoepitaxy of (010) β-Ga_2O_3 by Metalorganic Vapor Phase Epitaxy: Expanding the Growth Window. *Appl. Phys. Lett.* **2020**, *117* (14), 142102.

(61) Rajapitamahuni, A. K.; Thoutam, L. R.; Ranga, P.; Krishnamoorthy, S.; Jalan, B. Impurity Band Conduction in Si-Doped-Ga_2O_3 Films. *Appl. Phys. Lett.* **2021**, *118* (7), 072105.

(62) Lee, K. H.; Kang, M. S.; Zhang, S. P.; Gu, Y. Y.; Lodge, T. P.; Frisbie, C. D. Cut and Stick" Rubbery Ion Gels as High Capacitance Gate Dielectrics. *Adv. Mater.* **2012**, *24* (32), 4457−4462.

(63) Ghosh, K.; Singisetti, U. Electron mobility in monoclinic β-Ga_2O_3 Effect of Plasmon-Phonon Coupling, Anisotropy, and Confinement. *J. Mater. Res.* **2017**, *32* (22), 4142−4152.